Available online at www.sciencedirect.com
SCIENCE DIRECT®
Journal of Solid State Chemistry 172 (2003) 219–231
JOURNAL OF SOLID STATE CHEMISTRY
http://elsevier.com/locate/jssc

Electron/hole and ion transport in $La_{1-x}Sr_xFeO_{3-\delta}$

M.V. Patrakeev,[a] J.A. Bahteeva,[a] E.B. Mitberg,[a] I.A. Leonidov,[a] V.L. Kozhevnikov,[a,*] and K.R. Poeppelmeier[b]

[a] *Institute of Solid State Chemistry, Ural Division of RAS, Pervomaiskaia 91, Ekaterinburg 620219, Russia*
[b] *Northwestern University, Department of Chemistry, 2145 Sheridan Road, Evanston IL-60208, USA*

Received 11 September 2002; received in revised form 10 December 2002; accepted 15 December 2002

Abstract

The conductivity of the entire solid solution $La_{1-x}Sr_xFeO_{3-\delta}$, where x =0.2, 0.4, 0.5, 0.7 and 0.9, in the oxygen partial pressure range 10^{-19}–0.5 atm and temperatures between 750°C and 950°C is reported. The partial contributions from different charge carriers and the energetic parameters governing transport of charged species reveal that the lanthanum–strontium ferrites can be characterized as mixed, ion–electron conductors in the low oxygen pressure/high oxygen deficiency limit. The partial contributions to conductivity from oxygen ions, electrons and holes increase with strontium content and attain maximal values at x =0.5. Further increase in doping results in development of oxygen vacancy ordering phenomena and deterioration of conducting properties.

Keywords: Lanthanum–strontium ferrite; Oxygen conductivity; Oxygen ordering; Electron conductivity

1. Introduction

The lanthanum–strontium ferrite solid solution $La_{1-x}Sr_xFeO_{3-\delta}$ has been intensively studied. This interest is related to the potential of these oxides for such applications as catalysts, high-temperature fuel cell electrodes and membrane materials. Features of the crystalline structure and peculiarities of the defect state of these materials have been reported rather extensively [1–12]. At the same time, a number of controversies exist concerning the transport properties. For example, Mizusaki et al. [1,2] analyzed their data for conductivity in oxides with x =0, 0.1 and 0.25 assuming only an electronic component. Later Teraoka et al. [3] reported a high semi-permeability of oxygen, thus evidencing considerable oxygen-ion contribution to the conductivity in ferrites with large strontium content. In contrast, Kim et al. [10] supposed negligibly small ion contribution in their analysis of conductivity in specimens with x =0.6 and 0.8. The studies by ten Elshof et al. [11,12] also demonstrated appreciable oxygen semi-permeability, i.e. oxygen ion contribution to the conductivity, in oxides with x =0.1–0.4. Overall, considerable disagreement exists on the magnitude of the ion component in the conductivity. Moreover, most papers on transport properties involve relatively narrow concentration limits where either minimal strontium or strontium-rich compositions were studied. In addition, given the different temperatures and oxygen pressure intervals utilized, it is difficult to make a comparison of the results which have been reported and to delineate the influence of the acceptor doping upon transport parameters over the entire range of the solid solution. Also, the ion conductivity was measured mainly in the high-pressure extreme, while data at low partial pressure of oxygen remain scarce. The present work was directed, therefore, at studying the influence of acceptor doping on the high-temperature conductivity in $La_{1-x}Sr_xFeO_{3-\delta}$, where x =0.2, 0.4, 0.5, 0.7 and 0.9, over a wide range of oxygen partial pressures. Particular attention is given to the data analysis below 10^{-6} atm.

2. Experimental

The samples used in this study were prepared by solid-state reaction. Starting materials were oxides Fe_2O_3

*Corresponding author. Fax: +7-3432-74-00-03.
E-mail address: kozhevnikov@imp.uran.ru (V.L. Kozhevnikov).

0022-4596/03/$ - see front matter © 2003 Elsevier Science (USA). All rights reserved.
doi:10.1016/S0022-4596(03)00040-9

(99.2%), La_2O_3 (99.96%) and strontium carbonate $SrCO_3$ (99.94%). The raw materials were pre-calcined to remove adsorbates, weighed in desirable amounts and thoroughly mixed with a mortar and pestle with addition of ethanol. The mixtures were pressed into pellets and fired at 750–1300°C in air. The materials were crushed into powder, pressed and fired several times with a gradual increase in temperature before single-phase specimens were obtained. Phase purity and determination of the lattice parameters were carried out with X-ray powder diffraction ($\lambda = 1.54178$ Å). The reduction experiments and studies of oxygen content changes in the specimens as a function of temperature were carried out with a Setaram TG-DTA-92 thermoanalyzer in the atmosphere containing 5% H_2 and 95% He. The residual water vapor in the gas mixture was frozen with liquid nitrogen before passing the gas into the thermoanalyzer. The reduction process was carried out until the sample weight was constant indicating complete reduction of the ferrite into iron metal, SrO and La_2O_3. The respective weight loss was used to calculate oxygen content in the starting ferrite.

A part of the synthesized materials was ball-milled in ethanol media and pressed into discs under 2 kbar uniaxial load. The disks were sintered in air at 1300–1350°C for 10 h to a density no less than 90% of theoretical. Rectangular bars $2 \times 2 \times 15\,mm^3$ were cut from the sintered discs for the four-probe d.c. conductivity measurements. Potential probes and current leads were made of the 0.3 mm Pt wire and tightly wound to the specimen with 7 and 12 mm spacing, respectively. The wired specimen was sealed under atmosphere containing 50% O_2 and 50% CO_2 in the measuring cell of cubically stabilized zirconia. The cell was equipped with two pairs of Pt electrodes. One pair was used as oxygen pump in order to change and maintain oxygen partial pressure (pO_2) while the other was utilized as oxygen sensor in order to independently control the pO_2 inside the cell. The assembly was set in the isothermal zone of a tubular furnace where the temperature of the experiment was maintained. The electrical parameters were measured with a high-precision voltmeter Solartron 7081. Computer-controlled operation of the oxygen pump and sensor provided precise variation and maintenance of the partial oxygen pressure in the cell. The measurements were carried out in the mode of decreasing oxygen partial pressure in isothermal runs. The relaxation time after a change in the oxygen pressure over a sample varied and was dependent on the temperature and oxygen partial pressure range. The criterion for achieving equilibrium was accepted a relaxation rate less than 0.1% per minute in the logarithm of the conductivity while at fixed oxygen pressure inside the cell.

3. Results and discussion

3.1. Crystal structure and oxygen content

The X-ray powder diffraction patterns of the as-synthesized samples $La_{1-x}Sr_xFeO_{3-\delta}$ show the formation of perovskite-like structures at all strontium contents, Fig. 1. In agreement with previous reports [6,13] the crystal lattices correspond to orthorhombic, rhombohedral and cubic symmetry for specimens with $x = 0.2$; 0.4, 0.5 and 0.7; 0.9, respectively. The unit cell parameters are shown in Table 1. The oxygen content changes on heating in a 5% H_2:95% He atmosphere are shown in Fig. 2. Most of the reduction occurs by 500°C. At the same time, the weight changes are small in the temperature range 500–750°C where oxygen content remains close to $(3-\delta) \approx 3 - x/2$. The X-ray powder diffraction patterns of the samples, after cooling from 700°C in the TG apparatus, are given in Fig. 3. Heating to still higher temperatures initiates further loss of oxygen and partial reduction of iron to the +2 oxidation state, which results in formation of oxygen-deficient oxides $La_{1-x}Sr_xFe^{3+}_{1-2\delta}Fe^{2+}_{2\delta}O_{3-x/2-\delta}$ and then to the loss of stability and structural collapse.

The sample with $x = 0.2$ retains an orthorhombic perovskite-like structure after firing at 700°C in the harshly reducing hydrogen–helium mixture as can be seen from Fig. 3. The X-ray reflections can be indexed with a rhombohedral unit cell for $x = 0.4$ and 0.5. The oxygen vacancies appear to be randomized in the composition range $x \leqslant 0.5$. Quite differently, the compound with $x = 0.7$ acquires an orthorhombic triple perovskite structure where oxygen vacancies order to form layers of iron–oxygen tetrahedra (T) alternating along the *b*-axis with the layers of iron–oxygen

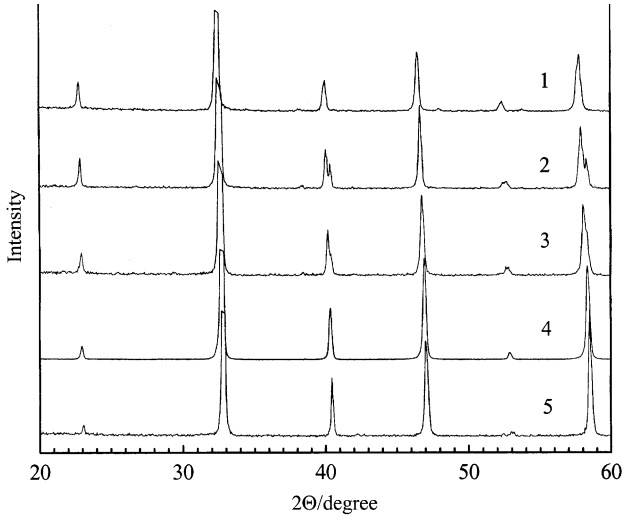

Fig. 1. The X-ray powder diffraction patterns (Cu$K\alpha$ radiation) for the as-synthesized in air samples of $La_{1-x}Sr_xFeO_{3-\delta}$, where $x = 0.2$ (1), 0.4 (2), 0.5 (3), 0.7 (4) and 0.9 (5).

Table 1
Unit cell data at room temperature for specimens $La_{1-x}Sr_xFeO_{3-\delta}$ equilibrated at 950°C and quenched in air

x	Symmetry	a(Å)	b(Å)	c(Å)
0.2	Orthorhombic	5.523(1)	5.550(1)	7.817(2)
0.4	Rhombohedral[a]	5.519(1)		13.420(3)
0.5	Rhombohedral	5.503(1)		13.417(3)
0.7	Cubic	3.873(1)		
0.9	Cubic	3.866(1)		

[a] Hexagonal setting.

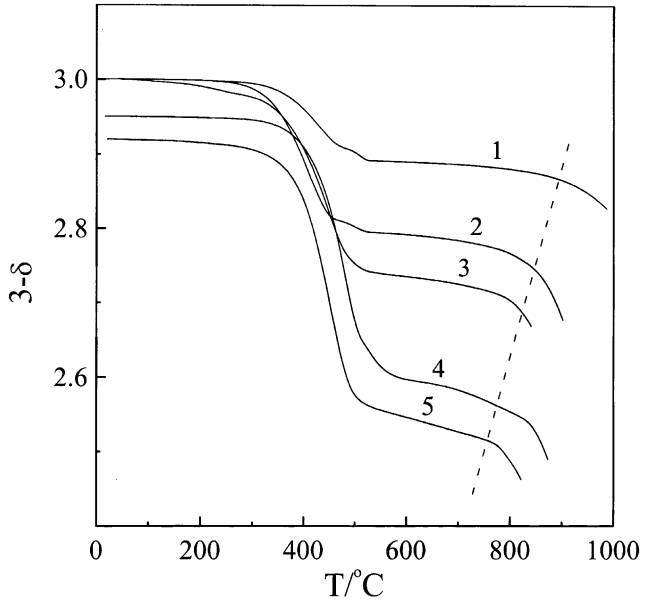

Fig. 2. The weight changes for $La_{1-x}Sr_xFeO_{3-\delta}$ at heating in the atmosphere containing 5% H_2 and 95% He; x =0.2 (1), 0.4 (2), 0.5 (3), 0.7 (4) and 0.9 (5). The dashed line shows approximately the decomposition temperature.

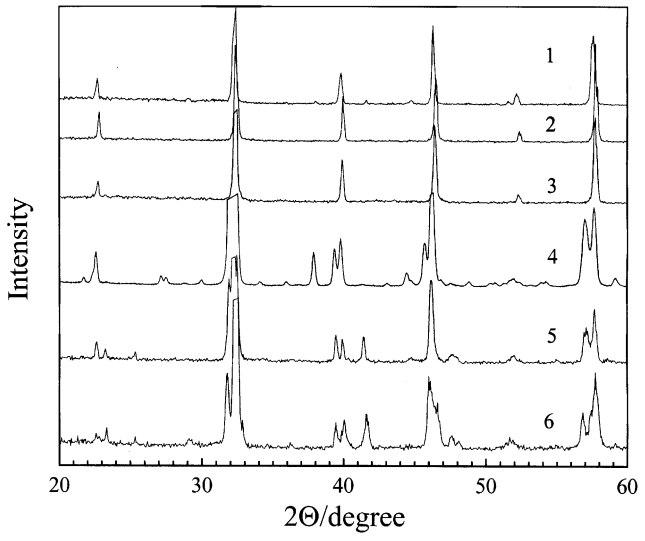

Fig. 3. The X-ray powder diffraction patterns (Cu$K\alpha$ radiation) for the samples of $La_{1-x}Sr_xFeO_{3-\delta}$ fired at 700°C in the atmosphere containing 5% H_2 and 95% He; x =0.2 (1), 0.4 (2), 0.5 (3), 0.7 (4), 0.9 (5) and 1.0 (6).

octahedra (O) as …OOTOOT… [14]. The diffraction pattern for $La_{0.1}Sr_{0.9}FeO_{2.55}$ is close to that of the brownmillerite-like ferrite $Sr_2Fe_2O_5$ where vacancy ordering results in the stacking sequence …OTOT… along the b-axis [15,16]. The respective unit cell parameters are given in Table 2.

3.2. General trends in conductivity

The measured data, more precisely the logarithm of the total conductivity (σ) versus the logarithm of the oxygen partial pressure at different temperatures (T), are shown in Fig. 4 for the specimens $La_{1-x}Sr_xFeO_{3-\delta}$, where x =0.2, 0.4, 0.5, 0.7 and 0.9. It should be noted that the overall time necessary for carrying out measurements for one specimen takes about 200–300 h. In contrast to the other reports [2,10], where the temperature interval above 900°C was studied, the measurements in this study are in the range 750–950°C. At the same time, our results and those of others [2,10] are in good correspondence when the parameters T and pO_2 are the same and the doping levels are similar. The conductivity increase with pressure observed to the right of the minima of $\lg\sigma$ versus $\lg pO_2$ shows that the majority charge carriers are electron holes. Thus σ_p dominates the total conductivity in the high-pressure limit. The respective conductivity changes with pressure are nearly proportional to $pO_2^{+1/4}$. The increase in conductivity with the pressure decrease, which is seen to the left of the minima, is indicative of electron-like charge carrier contribution (σ_n) dominating the conductivity in the low-pressure extreme. The conductivity changes with pressure approach the $\sigma_n \sim pO_2^{-1/4}$ dependence.

Three distinctly different regions of the conductivity behavior can be observed. An example is given in Fig. 5 where the conductivity data at 850°C are shown for $La_{0.5}Sr_{0.5}FeO_{3-\delta}$ as collected at the oxygen pressure decrease (downward run) followed by the increase (upward run). Empty squares show results obtained under the equilibrium criterion as outlined in the experimental section. Perfect match of the data in the down- and upward runs is seen in the high-pressure range (III), where according to Fig. 4 the conductivity is metal-like, and in the low-pressure range (I), where according to Fig. 4 the conductivity is temperature activated as in a semi-conductor. Thus, in carrying out these experiments the equilibrium criterion is quite sufficient to measure the equilibrium conductivity data in the pressure ranges I and III. The conductivity appears to depend on pressure only weakly in the intermediate pressure range (II) where there is a considerable difference in the values obtained in the down- and upward runs. Filled squares in Fig. 5 show the data taken after equilibration for 5 h at every pressure point. It is seen that the differences become just

slightly smaller throughout the total measuring cycle at one temperature, which requires in excess of 200 h. The relaxation data at 850°C in Fig. 6 provide additional illustration with respect to the origin of this peculiar behavior. It is seen clearly from Fig. 6a that the equilibration kinetics is so slow in the pressure range II that the conductivity values continue to change after 5 h of equilibration time with practically the same rate as at the start of the experiment. Therefore, the conductivity data points obtained in the range II, even at very lengthy isochronous measurements, do not quite correspond to equilibrium values. This is also the situation when measurements are carried out under the accepted equilibrium criterion in the conditions where the drift in the logarithm of the conductivity, which can be calculated from Fig. 6a, is in fact as slow as 0.01–0.02% per minute. Therefore, in order to obtain conductivity data in the range II more close to equilibrium values more stringent equilibration criterion, for example, a relative drift in the logarithm of the conductivity of about 0.001% per minute or even smaller, would be required. However, the measuring cycle of the conductivity at any one selected temperature would have taken an unreasonably long time of many hundred hours. Quite in contrast, the equilibration time is relatively short in the pressure intervals I and III as is evidenced by the example shown in Fig. 6b; equilibrium is attained after reasonable equilibration times (0.5–3 h after which the conductivity becomes practically independent on time, i.e., the conductivity change with time becomes smaller than the equilibrium criterion). Having achieved this state, the computer stores into memory the respective value that can be interpreted as the equilibrium conductivity at the given external

Table 2
Unit cell data at room temperature for specimens $La_{1-x}Sr_xFeO_{3-\delta}$ equilibrated at 700°C and quenched in the gas mixture 5% H_2:95% He

x	Symmetry	a(Å)	b(Å)	c(Å)
0.2	Orthorhombic	5.535(1)	5.558(1)	7.838(2)
0.4	Rhombohedral[a]	5.500(1)		13.588(3)
0.5	Rhombohedral	5.509(1)		13.596(1)
0.7	Orthorhombic	5.498(1)	11.862(3)	5.569(1)
0.9	Orthorhombic	5.625(1)	15.743(3)	5.526(1)
1.0	Orthorhombic	5.672(1)	15.576(3)	5.528(1)

[a] Hexagonal setting.

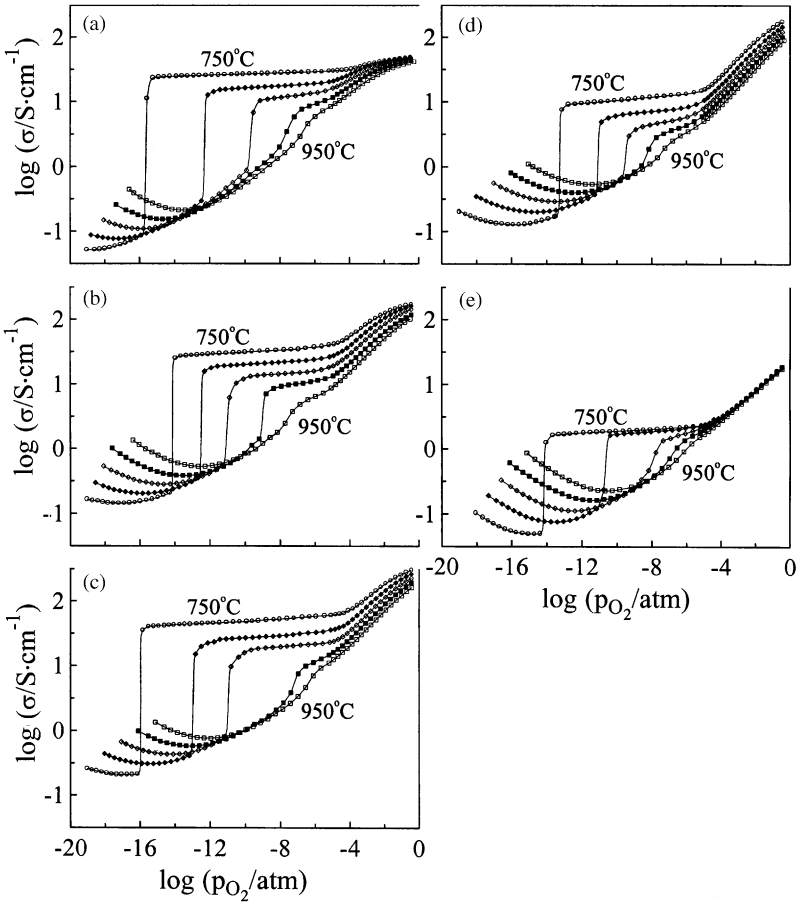

Fig. 4. The experimental results for changes in the total conductivity of $La_{1-x}Sr_xFeO_{3-\delta}$ with oxygen partial pressure at different temperatures; x =0.2 (a), 0.4 (b), 0.5 (c), 0.7 (d) and 0.9 (e). The temperature step between the isotherms is 50°C.

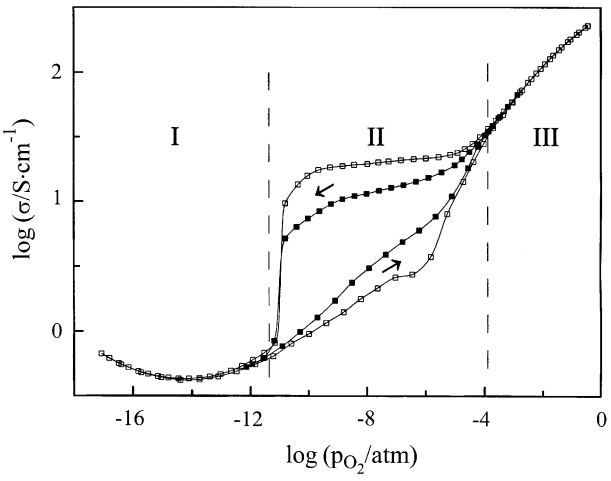

Fig. 5. The logarithmic plots of the conductivity versus oxygen partial pressure for $La_{0.5}Sr_{0.5}FeO_{3-\delta}$ at 850°C. Empty squares show results measured under the accepted equilibrium condition, i.e., the conductivity drift smaller than 0.01% per minute. Filled squares show results taken at isochronous measurements during 5 h at any given value of pressure. Arrows show direction of the pressure changes during measurements.

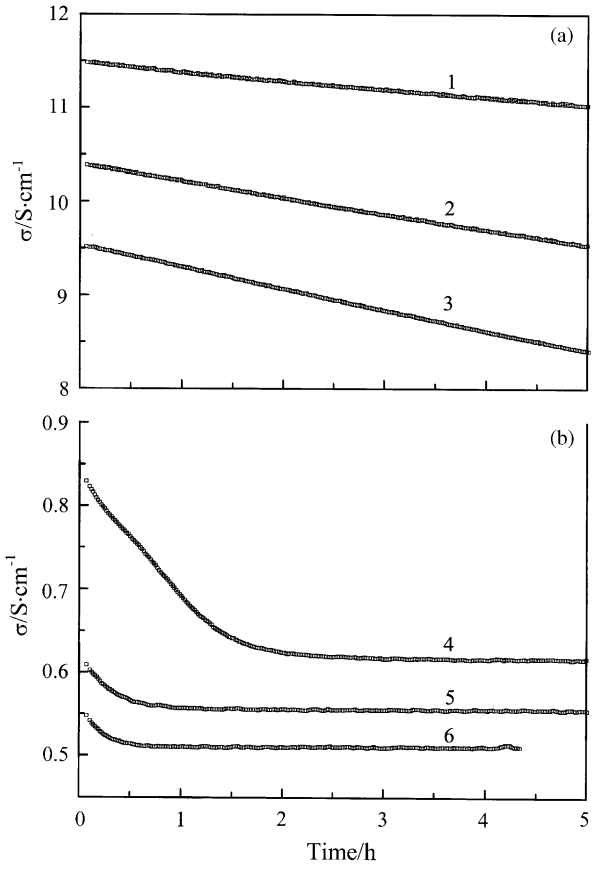

Fig. 6. The conductivity relaxation at the oxygen partial pressure decrease from 2.5×10^{-N} to 1×10^{-N} atm; N =9 (1), 10 (2), 11 (3), 12 (4), 13 (5) and 14 (6). (a) and (b) Relaxation in regions II and I in Fig. 5, respectively. The time necessary to change pressure in the measuring cell did not exceed 20–30 s at any selected pressure.

parameters T and pO_2. The very sluggish equilibration in the pressure range II may be related to the semiconductor to metal transition as proposed in studies [17,18]. However, there may be other processes such as diffusion related to phase boundaries, surface reactions, etc. More complete understanding of the oxygen equilibration kinetics in the intermediate pressure range deserves a separate investigation. Here we utilize only the data obtained in the low- and high-pressure intervals for the analysis of the equilibrium conductivity in the ferrites. Though limited to regions I and III, the obtained experimental results are nonetheless quite informative. For instance, the oxygen content in the ferrites strongly depends on oxygen pressure and temperature in the high-pressure limit. The respective changes can be determined relatively simply by making use of the TG measurements or coulometric titration technique, thus enabling an analysis of the conductivity changes with oxygen content as was done for $La_{0.3}Sr_{0.7}Fe_{1-x}Ga_xO_{3-\delta}$ [19].

This study is focused on the data analysis in the low-pressure range I. The conductivity minima of the isotherms in Fig. 4 correspond to near equality of the electron (σ_n) and hole (σ_p) contributions. It is important to notice that the conductivity changes with pressure near the minima are substantially smoother than expected from the sum of the electron and hole contributions only $\sigma=\sigma_n{}^{\circ}\,pO_2^{-1/4}+\sigma_p{}^{\circ}\,pO_2^{+1/4}$. This indicates the presence of one additional, pressure independent, contribution to the conductivity. Such a contribution in the ferrites under consideration is due to the electric current formed by the movement of oxygen ions. Therefore, the experimental data around the minima were approximated with the expression

$$\sigma(T,pO_2)=\sigma_i(T)+\sigma_n{}^{\circ}(T)\,pO_2^{-1/4}+\sigma_p{}^{\circ}(T)\,pO_2^{+1/4}, \quad (1)$$

where $\sigma_i(T)$ is pressure-independent oxygen ion contribution while coefficients $\sigma_n{}^{\circ}(T)$ and $\sigma_p{}^{\circ}(T)$ represent n- and p-type contributions, as extrapolated to $pO_2=1$ atm, respectively. The parameter values that give a satisfactory fit of Eq. (1) to the experimental data for different compositions and temperatures are summarized in Table 3. For example, a good match of the model calculations with the experimental data can be seen in Fig. 7 for $La_{0.6}Sr_{0.4}FeO_{3-\delta}$.

The ion conductivity at different temperatures (see Table 3) and experimental data for total conductivity (see Fig. 4) can be utilized to calculate the difference $\sigma(T,pO_2)-\sigma_i(T)\equiv\sigma_{n+p}(T,pO_2)$ that according to Eq. (1) corresponds to the sum of the electron and hole contributions. Examples in Fig. 8a and b show pressure variations in $\sigma_{n+p}(T,pO_2)$ at different temperatures for $La_{0.6}Sr_{0.4}FeO_{3-\delta}$ and at 950°C for different compositions, respectively. Comparison of the isotherms in

Table 3
The conductivity parameters σ_i(S cm^{-1}), σ_n°(S cm^{-1} atm$^{+1/4}$) and σ_p°(S cm^{-1} atm$^{-1/4}$) in Eq. (1) for $La_{1-x}Sr_xFeO_{3-\delta}$

x	Parameter	Temperature (°C)				
		950	900	850	800	750
0.2	σ_i	1.01×10^{-1}	7.75×10^{-2}	5.93×10^{-2}	4.68×10^{-2}	3.41×10^{-2}
	σ_n°	2.31×10^{-5}	7.99×10^{-6}	2.56×10^{-6}	6.95×10^{-7}	1.61×10^{-7}
	σ_p°	134	176	236	316	467
0.4	σ_i	0.313	0.232	0.185	0.141	0.106
	σ_n°	8.04×10^{-5}	3.05×10^{-5}	1.05×10^{-5}	3.36×10^{-6}	9.5×10^{-7}
	σ_p°	146.3	178.6	220.8	283.4	365.1
0.5	σ_i	0.462	0.366	0.275	0.205	0.150
	σ_n°	1.42×10^{-4}	5.61×10^{-5}	2.05×10^{-5}	6.78×10^{-6}	1.79×10^{-6}
	σ_p°	161	202	284	369	458
0.7	σ_i	0.341	0.256	0.192	0.137	9.04×10^{-2}
	σ_n°	1.32×10^{-4}	5.38×10^{-5}	2.04×10^{-5}	6.64×10^{-6}	1.98×10^{-6}
	σ_p°	74.6	95.8	123	151	181
0.9	σ_i	1.24×10^{-1}	9.39×10^{-2}	6.14×10^{-2}	3.94×10^{-2}	2.34×10^{-2}
	σ_n°	1.23×10^{-4}	4.98×10^{-5}	1.95×10^{-5}	7.17×10^{-6}	2.41×10^{-6}
	σ_p°	22.3	25.3	33.4	46.1	69.4

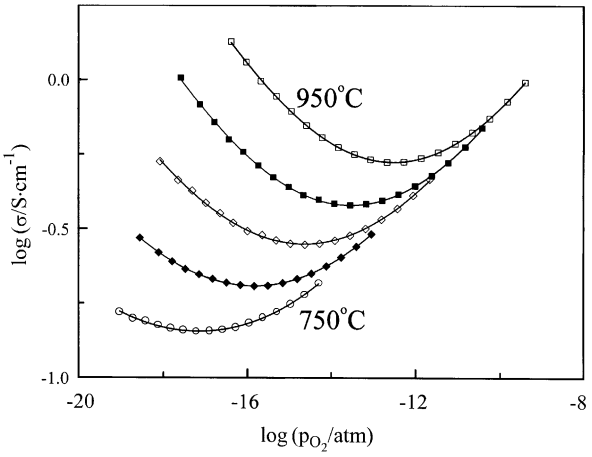

Fig. 7. The logarithmic dependencies of the conductivity versus oxygen partial pressure near the point of intrinsic electron disorder for $La_{0.6}Sr_{0.4}FeO_{3-\delta}$ at different temperatures. Solid lines show calculation results. The temperature step between the isotherms is to 50°C.

Figs. 8a and 4b demonstrates their similar shape. This is not surprising and should be expected because deduction of the constant ion contribution from the respective isotherms in Fig. 4 results mainly in more distinct, sharp outline of the isotherms' minima and, moreover, in the downward shift of the isotherms along the $\log\sigma$ axis. One may notice also from Fig. 8 that the intersection of the straight lines that approximate the σ_n and σ_p legs of the isotherms to the left and right of the minima $\left(\sigma_{n+p}^{min}\right)$, respectively, gives values very close to $\sigma_{n+p}^{min}/2$. This is an additional justification of our correct separation of the

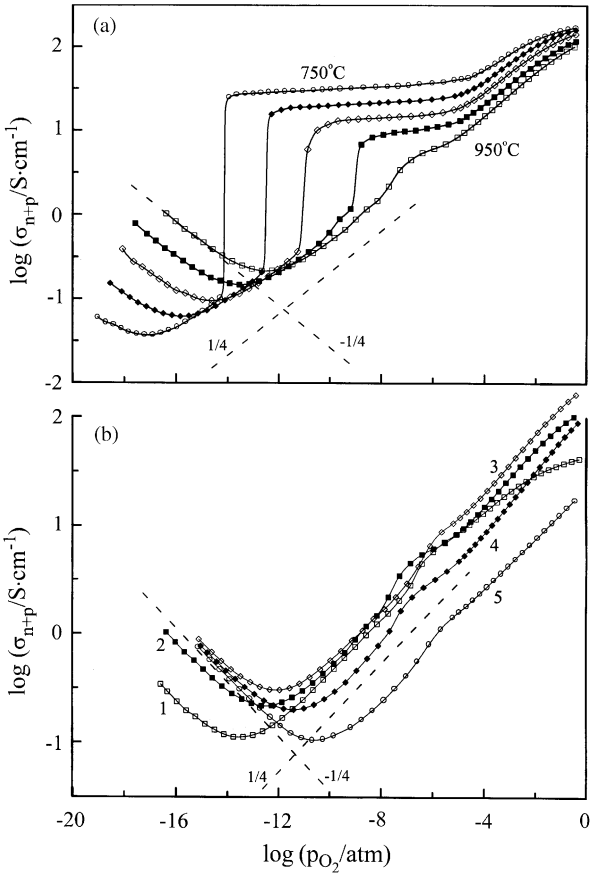

Fig. 8. The isothermal logarithmic plots for the sum of electron and hole contributions versus oxygen partial pressure. (a) $La_{0.6}Sr_{0.4}FeO_{3-\delta}$ at different temperatures; (b) $La_{1-x}Sr_xFeO_{3-\delta}$ at 950°C where x =0.2 (1), 0.4 (2), 0.5 (3), 0.7 (4) and 0.9 (5). Dashed lines show slopes corresponding to pressure dependencies $pO_2^{\pm1/4}$.

electron–hole contribution from the total conductivity. Generally, the above analysis demonstrates that there is an appreciable ion (oxygen) contribution to the total conductivity in $La_{1-x}Sr_xFeO_{3-\delta}$ when the activity of oxygen in gas phase is low. The ion conductivity σ_i, n-type conductivity σ_n at 10^{-16} atm and the minimal conductivity σ_{n+p}^{min} are shown with Arrhenius coordinates in Fig. 9. Straight lines can approximate all the data, which enables the calculation of the respective activation energies shown in Table 4.

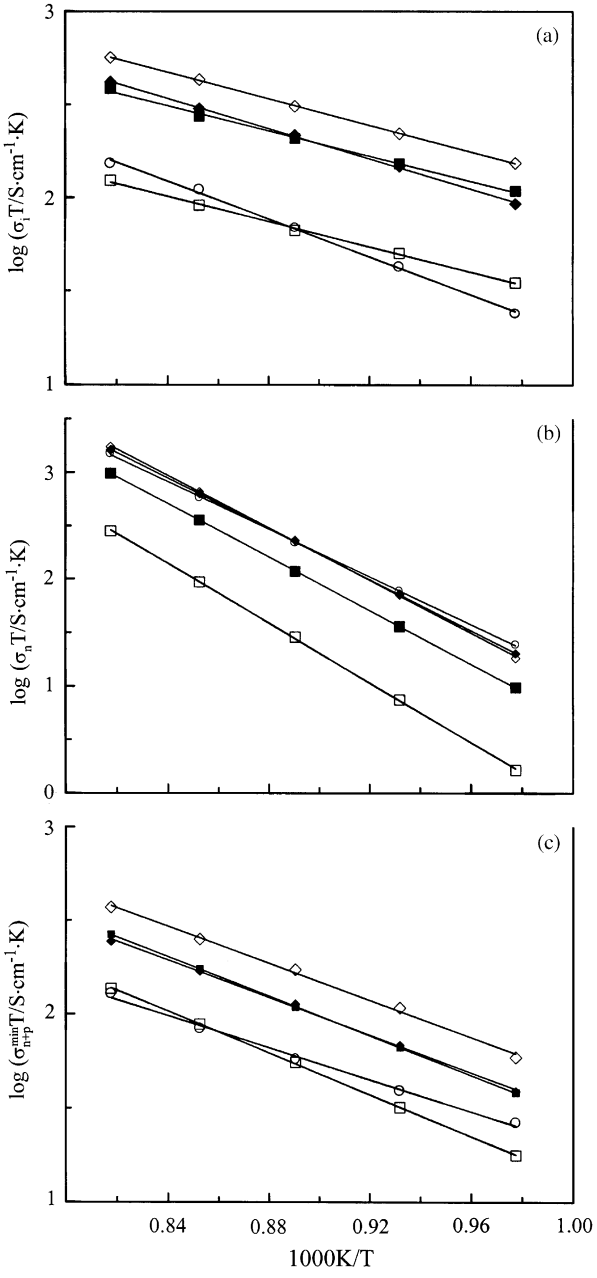

Fig. 9. Arrhenius plots for the ion conductivity (a), electron conductivity at 10^{-16} atm (b) and for the minimal electron–hole conductivity (c). x =0.2 (□), 0.4 (■), 0.5 (◇), 0.7 (◆) and 0.9 (○).

Table 4
The activation energies for the ion (E_i) and electron (E_n) contributions and for the minimal electron–hole conductivity (E_{min}) as calculated from plots $\ln(\sigma T)$ versus $1/T$

X	E_i(eV)	E_n(eV)	E_{min}(eV)
0.2	0.67	2.76	1.1
0.4	0.67	2.48	1.04
0.5	0.7	2.43	0.98
0.7	0.8	2.36	0.99
0.9	1.0	2.21	0.84

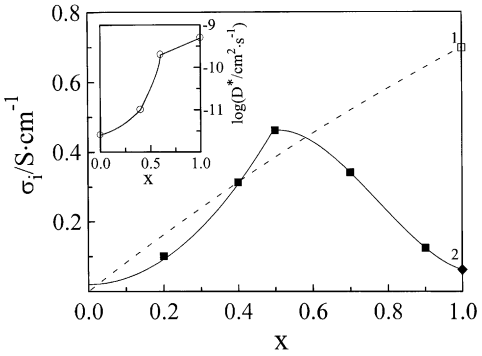

Fig. 10. The ion conductivity changes with strontium content in $La_{1-x}Sr_xFeO_{3-\delta}$ at 950°C. The results shown with symbols (◆) and (□) for the composition with x =1 are taken from works [17] and [20], respectively. The dashed line shows approximation of the experimental data at x =0.2, 0.4 and 0.5 by the function $\sigma_i = \sigma^\circ(3 - x/2)(x/2)$. The inset shows the data for the oxygen self-diffusion coefficient from work [9].

3.3. Oxygen ion conductivity

The data in Fig. 9a reveal that the ion conductivity attains a maximal value at x =0.5. Notice also that the apparent activation energy for the ion conductivity (E_i) does not depend on strontium content at $x \leqslant 0.5$, Table 4. Therefore, the acceptor content variations in this range do not effect the ion migration mechanism. This seems quite natural because all compositions at $x \leqslant 0.5$ have the same, perovskite-like structure. The ion conductivity dependence on strontium content $\sigma_i(x)$ is shown at 950°C in Fig. 10. The increase of $\sigma_i(x)$ with x in the range $x \leqslant 0.5$ generally follows the oxygen vacancy increase. One may suppose, therefore, that the average oxidation state of iron is close to +3 in the experimental conditions used or, in other words, the composition of ferrites with $x \leqslant 0.5$ remains close to the formula $La_{1-x}Sr_xFeO_{3-x/2}$ over the quite wide variations of oxygen activity in the pressure range I. This reasonable supposition corresponds to primarily ionic compensation of acceptors, and it seems to be quite relevant when the data are analyzed in the low oxygen pressures regime. The dashed line in Fig. 10 depicts the concentration-dependent behavior of $\sigma_{theor} = \sigma^\circ(3 - x/2)(x/2)$, where σ° is a constant, as fitted to experimental data at

$x = 0.2$, 0.4 and 0.5. This theoretical dependence reflects changes in ion conductivity with acceptor concentration in a perovskite lattice having $(x/2)$ random vacancies and $(3 - x/2)$ regular oxygen ions per elementary unit. The experimentally observed behavior generally follows this dependence at $x \leqslant 0.5$. Also, the line drawn over experimental points according to this dependence in the domain ($x \leqslant 0.5$) of the perovskite structure and then extrapolated to $x = 1$, gives the ion conductivity value in perfect match with the experimental result [20] obtained from permeation measurements at elevated temperatures and $pO_2 > 10^{-3}$ atm, i.e., in conditions where ferrite $SrFeO_{3-\delta}$ has considerable oxygen deficiency ($\delta \to 0.5$) and simultaneously retains the structure of an oxygen vacancy disordered perovskite [21,22]. The consistency of the ion conductivity values obtained by different methods in perovskite-like materials of $La_{1-x}Sr_xFeO_{3-\delta}$, in the low- and in the high-pressure limits, confirms the reliability of our approach, which we have utilized in the determination of the ion contribution. Also, it demonstrates that the ion conductivity in the ferrites at a given temperature does not depend on oxygen pressure and is defined mainly by the oxygen vacancy concentration as long as the vacancies remain disordered.

It is shown above that oxygen vacancy ordering in oxides with $x > 0.5$ results in formation of layered structures characterized by alternation of iron–oxygen octahedra and tetrahedra in $La_{0.3}Sr_{0.7}FeO_{2.65}$ and $La_{0.1}Sr_{0.9}FeO_{2.55}$. It can be noticed that the ratio of octahedrally coordinated iron to tetrahedrally coordinated iron is larger in $La_{0.3}Sr_{0.7}FeO_{2.65}$ than in $La_{0.1}Sr_{0.9}FeO_{2.55}$. It is known also that oxygen ion transport in vacancy-ordered ferrites develops mainly in the layers of octahedra over vacancies (V_{oct}) formed as a result of anti-Frenkel disordering $O^{2-}_{oct} + V_{tet} \leftrightarrow V_{oct} + O^{2-}_{tet}$ of oxygen anions in the layers of octahedra (O^{2-}_{oct}) and structural vacancies (V_{tet}) in the layers of tetrahedra [17,18]. Hence, the general decrease of the ion conductivity in compositions with $x > 0.5$ compared to that in the oxide with $x = 0.5$ and the greater decrease in the oxide $x = 0.9$ than in $x = 0.7$, see Fig. 10, appear to be a natural consequence of their local structures. Additional data at 950°C [17] are given in Fig. 10 for the brownmillerite-like ferrite $SrFeO_{2.5}$ where the relative amount of the ordered vacancies is larger than in $La_{0.1}Sr_{0.9}FeO_{2.55}$. Therefore, it is not surprising that the ion conductivity is somewhat smaller in $SrFeO_{2.5}$ than in $La_{0.1}Sr_{0.9}FeO_{2.55}$. As a whole, the concentration-dependent ion conductivity $\sigma_i(x)$ in Fig. 10 demonstrates rather directly that an increase in the amount of random vacancies results in the increase of the ion conductivity level. At the same time, an increase in the vacancy concentration favors a tendency for the vacancies to order, which in turn results in their efficient removal for the oxygen transport. The tendency for the apparent activation energy to increase at $x > 0.5$,

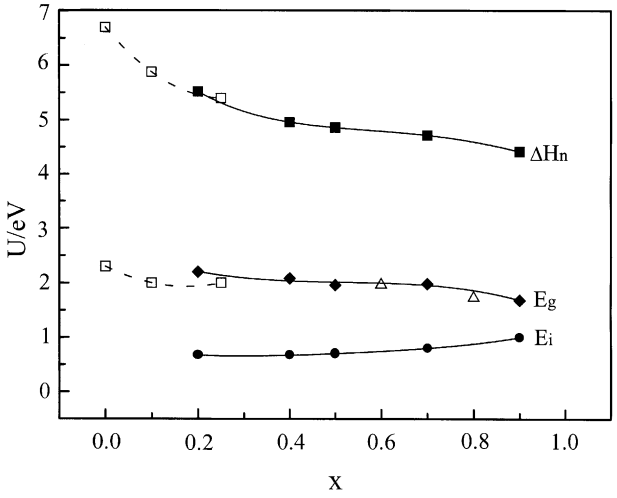

Fig. 11. Changes with strontium content in the energetic parameters for the conductivity in $La_{1-x}Sr_xFeO_{3-\delta}$. Symbols (□) and (Δ) represent results from works [2] and [10], respectively.

which can be seen in Fig. 11, shows again that the thermally activated ion transport in the vacancy-ordered phases $La_{0.3}Sr_{0.7}FeO_{2.65}$ or $La_{0.1}Sr_{0.9}FeO_{2.55}$ evolves on a background of a simultaneously developing "order↔disorder" type process [23].

Yet another feature in Fig. 10 attracts attention. Namely, the ion conductivity decrease with $x \to 0$ is somewhat faster compared to the dependence $\sigma_{theor} = \sigma^{\circ}(3 - x/2)(x/2)$, which gives $\sigma_{theor} \sim x$ at small doping, while the experimentally observed behavior appears to follow more closely $\sigma_i \sim x^2$. In order to understand the reason for this deviation, it is important to recognize that along with the number of multipliers $(3 - x/2)$ and $(x/2)$, which directly show the amount of migrating ions and number of vacancies available for ion jumps, respectively, there is a characteristic probability per unit time ω for the ion to jump that enters with the coefficient $\sigma^{\circ} \sim \omega$ [24]. This probability depends on the size of the "bottleneck" that must be overcome for the ion to jump from a regular site to the nearby vacancy. In ABO_3 perovskites this narrow space is framed by one B-type cation and two A-type cations and it would appear to be invariable at first glance. However, formation of oxygen vacancies in the solid solution $La_{1-x}Sr_xFeO_{3-x/2}$ results in a decrease in the average coordination numbers for the La^{3+}, Sr^{2+} and Fe^{3+} cations and, therefore, to the proportional decrease of their average radii [25]. As a result, the average size of the "bottleneck" increases with vacancy concentration, i.e., with the doping level. Consequently, the jump probability must increase nearly proportional to the doping, that is $\omega \sim x$, and, therefore, changes in the ion conductivity follow a nearly parabolic dependence. These arguments are applied only to the case of random vacancies, which occur in the range $x \leqslant 0.5$.

Others [9] observed the same concentration-dependent behavior of the tracer diffusion coefficient D^* of oxygen in the ferrites with $x<0.6$, see inset in Fig. 10. Note that the tracer diffusion coefficient is related to the self-diffusion coefficient D as $D^*=fD$, where f is the correlation factor of about unity in a perovskite-like lattice. Thus, this similarity ensues from the Nernst–Einstein relation that establishes the linear relation of the kinetic coefficients D and σ. At larger strontium content the diffusion coefficient [9] tends to slightly increase with x while ion conductivity decreases. This apparent controversy appears because the data reported previously [9] are obtained at high oxygen pressure ($pO_2\approx 0.05$ atm) when strontium-rich ferrites adopt perovskite-like structures with random vacancies. The results in the present work are obtained at low oxygen pressure when the vacancy concentration achieves such large values that strontium-rich ferrites exhibit vacancy ordering and deterioration of the ion transport. Notice additionally that our values $E_i\approx 0.7$ eV for the activation energy of the ion conductivity at $x\leqslant 0.5$ are very close to those for the diffusion activation energy at $x<0.6$ [9]. At larger strontium content the conductivity activation energy $E_i\approx 0.8$–1.0 eV, Table 4, exceeds slightly the diffusion activation energy (~ 0.8 eV) reported [9]. This difference is related apparently to the vacancy ordering↔disordering effects that develop at low oxygen pressure, even at rather high temperatures, and strongly influence the ion conductivity in strontium-rich ferrites.

3.4. p-type electronic conductivity

The conductivity increase with the pressure right to the minima, which can be seen, e.g., in Fig. 8b, reflects formation of holes at oxygen incorporation in the structure $1/2O_2\leftrightarrow O^{2-}+2h^+$. The respective equilibrium constant is

$$K_p=\frac{[h^+]^2[O^{2-}]}{pO_2^{1/2}}=K_p^{\circ}\exp(-\Delta H_p/kT), \qquad (2)$$

where K_p° is a constant independent of the temperature and ΔH_p is the reaction enthalpy. The oxygen content in the ferrites is essentially independent of the oxygen pressure near the minima, i.e., in the low-pressure extreme, and is defined mainly by the acceptor content, $[O^{2-}]\approx 3-x/2=\text{const}$. In fact, this relation represents the electroneutrality requirement when changes in electric charge of the crystal lattice caused by the introduction of acceptors are compensated by the appearance of oxygen vacancies. This ionic compensation mechanism of maintaining electrical neutrality of the crystal lattice is well known [26]. At this condition, the pressure dependence of the hole conductivity $\sigma_p\sim[h^+]\sim pO_2^{1/4}$ follows from the equilibrium constant in general correspondence with the experiment. Small humps on the isotherms between 10^{-8} and 10^{-4} atm in Fig. 8b appear to be a result of not reaching equilibrium in this pressure range as discussed above. Also, some deviations from strict proportionality $\sigma_p\sim pO_2^{1/4}$, more noticeable at small x's, can also be seen at $pO_2>10^{-4}$ atm. These deviations possibly reflect that purely ionic compensation of acceptors becomes a poor approximation of the electroneutrality requirement at high enough pressure [27]. The increase of the parameter σ_p° in Eq. (1) and of the experimental values σ_p with the temperature decrease at high pressures of oxygen indicate the exothermal nature of the oxygen incorporation reaction. Evaluation of ΔH_p from the experimental data gives an estimation of about ~ 1 eV, which is in favorable correspondence with the partial enthalpy reported previously [5].

In the high-pressure limit, where oxygen deficiency tends to approach a small value $\delta\to 0$ [4], the conductivity increase with strontium content within $0\leqslant x\leqslant 0.5$ in Fig. 12a may possibly be a consequence of the change in the compensation mechanism of acceptors from ionic, which dominates in the low-pressure range, to an electronic one in correspondence with the substitution scheme $La^{3+}+Fe^{3+}=Sr^{2+}+Fe^{4+}$. With these conditions, the electroneutrality

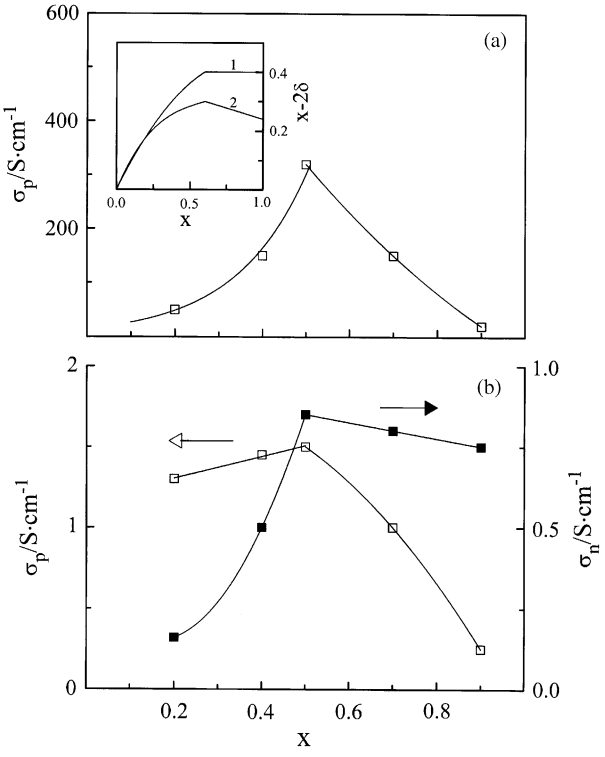

Fig. 12. Changes in the hole and electron contributions to conductivity with strontium content in $La_{1-x}Sr_xFeO_{3-\delta}$. (a) σ_p at $pO_2=0.21$ atm and $T=750^{\circ}C$. The inset shows changes with x in the concentration of holes calculated as $x-2\delta$ at 700°C (1) and 900°C (2) from the data in work [4]. (b) σ_p and σ_n at 950°C and $pO_2=10^{-8}$ and 10^{-15} atm, respectively.

requirement is satisfied as a result of formation of electronic defects only [26] and the concentration of electron holes is equal to the concentration of acceptors. Assuming electronic compensation and polaron type conduction, the conductivity is expected to change with the doping as $\sigma_p \sim x(1-x)$, where multipliers x and $(1-x)$ represent the number of holes (Fe^{4+} cations) and positions available for the holes (Fe^{3+} cations), respectively [28]. This relation results in a linear increase of the conductivity with acceptor content at small x's. It follows, however, from the experiment that the conductivity changes nearly as $\sigma_p \sim x^2$ in the range $0 \leqslant x \leqslant 0.5$, see Fig. 12a. Thus, the multiplier that corresponds to the contribution of the hole mobility in conductivity must change with x in a more complex fashion than it is often presumed, i.e., $\mu_p \sim (1-x)$. This observation can be explained in a manner similar to the one used previously in the discussion of the ion conductivity. Briefly, it is well known that the hole transport in many complex iron oxides occurs as a result of thermally activated jumps of electron holes from Fe^{4+} cations to nearby Fe^{3+} cations via the intermediate (bridging) oxygen anions. This suggests that the possibility for the hole to temporarily jump on an oxide anion is defined, along with other factors, by the Coulomb interaction of the hole with the nearest neighbors of the anion O^{2-} in the A-sublattice, i.e., with the La^{3+} and Sr^{2+} cations. This repulsive interaction is minimal when only Sr^{2+} cations surround the oxygen anion and it is maximal when all four neighbors bear a larger positive charge, i.e., when they are La^{3+} cations. Therefore, partial replacement of lanthanum for strontium results in the decrease of the Coulomb repulsion roughly proportional to the strontium content, resulting in a proportional increase of the probability for holes to successfully jump along the $\ldots Fe^{4+} \rightarrow O^{2-} \rightarrow Fe^{3+} \ldots$ chains. Recall that this probability enters the hole mobility [28] along with the multiplier $(1-x)$ thus giving the overall dependence for the mobility as $\mu_p \sim x(1-x)$ or $\mu_p \sim x$ at small x's. Thus, the conductivity, where there is one more multiplier x related to concentration of holes, may indeed change proportionally to x^2. The explanation above involves the jump probability, which is often considered as a constant. However, this may not necessarily be accurate if the composition of the A-sublattice changes considerably.

The acceptor concentration-dependent behavior of σ_p in the high-pressure extreme changes when $x > 0.5$. The hole conductivity decreases in this range with the acceptor concentration increase. This change may possibly indicate a shift from purely electronic to the mixed, ionic–electronic compensation when the concentration of acceptors becomes sufficiently large. In the mixed regime, changes in the concentration of holes, number of acceptors and the oxygen non-stoichiometry are interrelated with $[h^+] = x - 2\delta$. It follows from an earlier experiment [4] that the value of δ at a given temperature depends on x, and this dependence indeed results in the maximal concentration of holes near $x \approx 0.5$ as seen from the inset in Fig. 12a. However, the hole concentration decrease at $x > 0.5$ is much less pronounced than the conductivity decrease. Hence, we should conclude that the changes in the conductivity at $x > 0.5$ reflect mainly the mobility decrease of holes, which likely is due to the extensive accumulation of oxygen vacancies. The decrease in the mobility overpowers any enhancement caused by the increase in strontium content.

The hole conductivity in the low-pressure limit is considerably smaller than in the high-pressure extreme and it slightly, almost linearly increases with strontium content at $x \leqslant 0.5$, Fig. 12b. In this range of pressure, where compensation of acceptors is primarily ionic, the concentration of holes (and electrons) is regulated mainly by temperature and the value of the forbidden gap (see below). It does not depend essentially on the concentration of acceptors. Therefore, the conductivity increase possibly reflects an increase in the mobility of holes with strontium content because of the decrease in the Coulomb repulsion. On the other hand, oxygen vacancies that abundantly appear in the structure in the low-pressure limit disrupt transport in the $\ldots Fe^{4+} \rightarrow O^{2-} \rightarrow Fe^{3+} \ldots$ chains and, thus, assist in the strong suppression of the hole mobility. As a result, the conductivity increase with x is much less profound than in the high-pressure range, where the concentration of vacancies is always relatively small. Further increase in the strontium content (when oxygen pressure is small) favors formation of vacancy-ordered structures characterized by alternation of layers of iron–oxygen octahedra and tetrahedra when $x > 0.5$. It should be noticed here that electronic carriers move mainly in the layers of octahedra [17,18] and the number of such "conducting" layers becomes smaller when strontium content increases. This structural rearrangement may help to explain the general decrease in the conductivity with increasing strontium ($x > 0.5$) as seen in Fig. 12b.

3.5. *n-type electronic conductivity*

The appearance of n-type carriers in the ferrites as the oxygen pressures decrease is related to partial loss of the lattice oxygen on heating, $O^{2-} \leftrightarrow 1/2O_2 + 2e^-$. The respective equilibrium constant is given by

$$K_n = \frac{[e^-]^2 pO_2^{1/2}}{[O^{2-}]} = K_n^{\circ} \exp(-\Delta H_n / kT), \quad (3)$$

where K_n° is a constant independent on temperature and ΔH_n is the reaction enthalpy. At low oxygen pressures, when ionic compensation of acceptors dominates, as

described above, the proportionality $\sigma_n \sim [e^-] \sim pO_2^{-1/4}$, which is consistent with the experiment, immediately follows from Eq. (3) if the mobility of the electrons is a constant. Also, the activation energy for n-type conductivity, E_n, should be approximately equal to $\Delta H_n/2$ if the mobility activation energy is small compared to the enthalpy of oxygen depletion. Values of E_n for different strontium contents were calculated from plots of $\lg(\sigma_n T)$ versus $1/T$ at $pO_2 = 10^{-16}$ atm, Table 4. The concentration-dependent behavior of the calculated enthalpy $\Delta H_n \approx 2E_n$ illustrated in Fig. 11 is in good agreement with a previous study [2]. From Fig. 11 it can be seen clearly that the oxygen depletion enthalpy at low oxygen pressure increases with the lanthanum content across the solid solution. This trend can explain the decrease in the electron contribution (σ_n) with the increase in lanthanum content in oxides with $x \leqslant 0.5$, Fig. 12b. A relatively weak dependence of σ_n on the dopant content at $x > 0.5$ in Fig. 12b may possibly reflect a competition of two processes that simultaneously impact n-type contribution, i.e., some increase in the concentration of n-type carriers with x because of the decrease in ΔH_n, Fig. 11, and the decrease in the mobility of the carriers because of the vacancy ordering.

The forbidden energy gap E_g separating electron and hole carriers in the ferrites can be evaluated from the Arrhenius plots for the minimal conductivity [10] by the using of the relation

$$K_i = K_i^\circ \exp(-E_g/kT) = \left(\frac{\sigma_{n+p}^{min}}{2e(\mu_n \mu_p)^{1/2}} \right)^2, \quad (4)$$

where K_i is the equilibrium constant for the intrinsic disordering $0 \leftrightarrow e^- + h^+$, while symbols μ_n and μ_p designate mobility of n- and p-type carriers, respectively. It is known that activation energies are close to zero for mobilities of both electrons and holes in compositions with $x \leqslant 0.25$ [1,2]. If this holds true at larger strontium contents, the values of E_g in Fig. 11 can be calculated from Eq. (4) as $E_g = 2E_{min}$, where E_{min} is the activation energy for the minimal conductivity σ_{n+p}^{min}, Table 4. The results from others [2,10] are also given for comparison. The one set of values [2] appear slightly smaller than our results at comparable strontium contents. This difference likely occurs because the ionic component was not considered. It is seen from Fig. 11 that the ion contribution is governed by the activation energy E_i, which is considerably smaller that the forbidden gap E_g. Therefore, the ion and electron–hole contributions to total conductivity may become quite comparable when conditions exist such that the concentrations of electrons and holes are minimal, i.e., near intrinsic equilibrium. Hence, the disregard of the ion contribution in the analysis of electron transport properties when these conditions exist results in underestimation of the gap value.

3.6. Oxygen permeation

The ion conductivity in Table 3 and the total conductivity in Fig. 4 can be utilized together to calculate the ion transference numbers t_i as a function of oxygen pressure at different temperatures. As an example the results are shown for 900°C in Fig. 13. The transference numbers are convenient for evaluation of the oxygen flux jO_2 through the membrane-like sample of a mixed conductor under a given difference of the oxygen pressure on opposite sides of the membrane. For this we need to use the known relation [29]

$$jO_2 = \frac{RT}{16F^2L} \int_{pO_2''}^{pO_2'} t_i(1 - t_i) \mathrm{d} \ln pO_2 (\mathrm{mol\ cm^{-2}\ c^{-1}}). \quad (5)$$

Here, symbols R and F denote the gas constant and Faraday's number, respectively, L is the membrane thickness while symbols pO_2' and pO_2'' represent oxygen partial pressure values at the opposing sides of the membrane. The using of Eq. (5) is justified when the oxygen flux is limited by the bulk diffusion of charge carriers. This condition is indeed well satisfied for the ferrite membranes with the thickness of more than several dozen microns [11]. The calculation results for $L = 0.1$ cm and $T = 900$°C are shown in Fig. 14. As argued earlier and now expected, the maximal flux should be and is observed for the composition with $x = 0.5$. The calculated values for jO_2 are in good accord with previous results [12]. As a final observation we notice that the flux can achieve values corresponding to about 2–5 cm^3/min of the oxygen permeate or up to

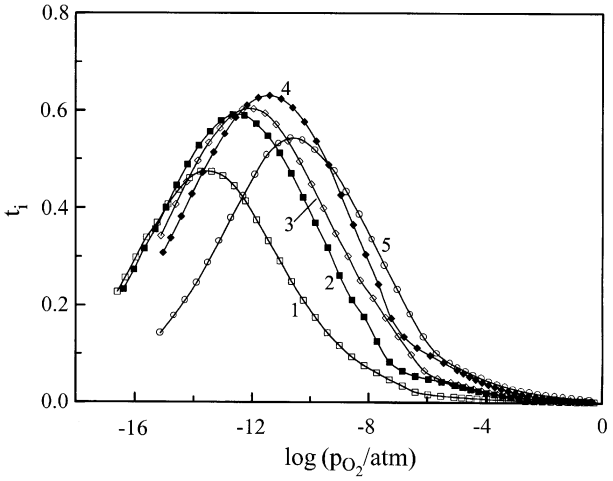

Fig. 13. The ion transference numbers in $La_{1-x}Sr_xFeO_{3-\delta}$ versus the logarithm of the oxygen partial pressure at 900°C. x =0.2 (1), 0.4 (2), 0.5 (3), 0.7 (4) and 0.9 (5).

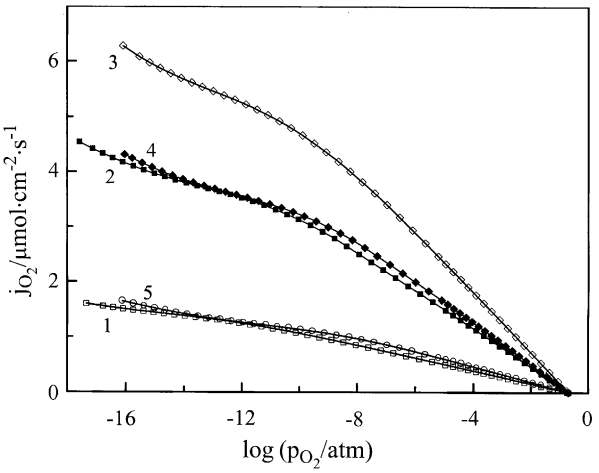

Fig. 14. The calculated oxygen fluxes through 1 mm thick membranes of $La_{1-x}Sr_xFeO_{3-\delta}$ at 900°C depending on the oxygen pressure at the low-pressure side. The oxygen pressure at the high-pressure side was accepted equal to 0.21 atm. x =0.2 (1), 0.4 (2), 0.5 (3), 0.7 (4) and 0.9 (5).

10–30 cm^3/min of syngas from 1 cm^2. The combination of the considerable oxygen semi-permeability with good thermodynamic stability favors the application of these ferrites in membrane type reactors for the methane partial oxidation.

Conclusions

Electrical conductivity measurements of the ferrites $La_{1-x}Sr_xFeO_{3-\delta}$, where x =0.2, 0.4, 0.5, 0.7 and 0.9, were performed in the oxygen partial pressure range 10^{-19}–0.5 atm and temperature varying between 750 and 950°C. The partial contributions of the oxygen-ion, electron- and hole-type charge carriers were derived from the analysis of the pressure dependencies of the total conductivity. The energetic parameters governing movement of the charge carriers were determined at different acceptor contents. Complementary to the known literature for the high-pressure limit, the mixed conductivity in the ferrites is shown to persist in the low-pressure extreme. It is argued that variations in the acceptor doping level and oxygen vacancy concentration result in structural modifications that develop simultaneously with changes in concentration and mobility of charge carriers. These results are used to evaluate the flux of oxygen through ferrite membranes. The demonstrated high efficiency of the oxygen separation and thermodynamic stability render these ferrites promising materials for use in membrane reactors employed in the partial oxidation of methane.

Acknowledgments

The work is carried out under the contract #01-03-96519 with Russian Foundation for Basic Research (RFBR). Authors appreciate partial support of this study by the Commission of RAS for young scientists under award #192 of the 6th competition-examination. One of us (K.R.P) is grateful to the EMSI program of the National Science Foundation and the U.S. Department of Energy Office of Science (CHE-9810378) at the Northwestern University Institute for Environmental Catalysis.

References

[1] J. Mizusaki, T. Sasamo, W.R. Cannon, H.K. Bowen, J. Amer. Ceram. Soc. 65 (1982) 363–368.
[2] J. Mizusaki, T. Sasamo, W.R. Cannon, H.K. Bowen, J. Amer. Ceram. Soc. 66 (1983) 247–252.
[3] Y. Teraoka, H.-M. Zhang, S. Furukawa, N. Yamazoe, Chem. Lett. (1985) 1743–1746.
[4] J. Mizusaki, M. Ychihiro, S. Yamauchi, K. Fueki, J. Solid State Chem. 58 (1985) 257–266.
[5] J. Mizusaki, M. Ychihiro, S. Yamauchi, K. Fueki, J. Solid State Chem. 67 (1987) 1–8.
[6] S.E. Dann, D.B. Currie, M.T. Weller, M.F. Thomas, A.D. Al-Rawwas, J. Solid State Chem. 109 (1994) 134–144.
[7] T. Ishigaki, S. Yamauchi, J. Mizusaki, K. Fueki, H. Naito, T. Adachi, J. Solid State Chem. 55 (1984) 50–53.
[8] T. Ishigaki, S. Yamauchi, K. Kishio, J. Mizusaki, K. Fueki, J. Solid State Chem. 73 (1988) 179–187.
[9] M.C. Kim, S.J. Park, H. Haneda, J. Tanaka, T. Mitsuhasi, S. Shirasaki, J. Mater. Sci. Lett. 9 (1990) 102–104.
[10] M.C. Kim, S.J. Park, H. Haneda, J. Tanaka, S. Shirasaki, Solid State Ionics 40/41 (1990) 239.
[11] J.E. ten Elshof, H.J.M. Bouwmeester, H. Verweij, Solid State Ionics 81 (1995) 97–109.
[12] J.E. ten Elshof, H.J.M. Bouwmeester, H. Verweij, Solid State Ionics 89 (1996) 81–92.
[13] P.D. Battle, T.C. Gibb, P. Lightfoot, J. Solid State Chem. 84 (1990) 271–279.
[14] P.D. Battle, T.C. Gibb, P. Lightfoot, J. Solid State Chem. 84 (1990) 237–244.
[15] J.-C. Grenier, N. Ea, M. Pouchard, P. Hagenmuller, J. Solid State Chem. 58 (1985) 243–252.
[16] M. Schmidt, S.J. Campbell, J. Solid State Chem. 156 (2001) 292–304, doi:10.1006/jssc.2000.8998.
[17] V.L. Kozhevnikov, I.A. Leonidov, M.V. Patrakeev, E.B. Mitberg, K.R. Poeppelmeier, J. Solid State Chem. 158 (2001) 320–326, doi:10.1006/jssc.2001.9120.
[18] I.A. Leonidov, V.L. Kozhevnikov, M.V. Patrakeev, E.B. Mitberg, K.R. Poeppelmeier, Solid State Ionics 144 (2001) 361–369.
[19] M.V. Patrakeev, E.B. Mitberg, A.A. Lakhtin, I.A. Leonidov, V.L. Kozhevnikov, V.V. Kharton, M. Avdeev, F.M.B. Marques, J. Solid State Chem. 167 (2002) 203–213, doi: 10.1006/jssc.2002.9644.
[20] Y. Teraoka, H.M. Zhang, S. Furukawa, N. Yamazoe, Chem. Lett. 7 (1988) 1084–1089.
[21] Y. Takeda, K. Kanno, T. Takada, O. Yamamoto, M. Takano, N. Nakayama, Y. Bando, J. Solid State Chem. 63 (1986) 237–249.
[22] J. Mizusaki, M. Okayasu, S. Yamauchi, K. Fueki, J. Solid State Chem. 99 (1992) 166–172.

[23] Y.A. Shilova, M.V. Patrakeev, E.B. Mitberg, I.A. Leonidov, V.L. Kozhevnikov, K.R. Poeppelmeier, J. Solid State Chem. 168 (2002) 275–283, doi: 10.1006/jssc.2002.9722.
[24] P.G. Shewmon, Diffusion in Solids, McGraw-Hill, New York, 1963.
[25] R.P. Shannon, Acta Crystallogr. A 32 (1976) 751–767.
[26] F.A. Kröger, The Chemistry of Imperfect Crystals, North-Holland, Amsterdam, 1964.
[27] N. Mansourian-Hadavi, T.O. Mason, D. Ko, K.R. Poeppelmeier, J. Solid State Chem. 164 (2002) 188–200, doi:10.1006/jssc.2001.9457.
[28] H.L. Tuller, in: R.C. Buchanan (Ed.), Ceramic Materials for Electronics, Marcel Dekker, INC., New York, 1986, p. 425.
[29] H. Schmalzried, Solid State Reactions, Verlag Chemie, Weinheim, 1981.